



HAL
open science

Diocahedral phyllosilicates versus zeolites and carbonates versus zeolites competitions as constraints to understanding early Mars alteration conditions

Jean-Christophe Viennet, Benjamin Bultel, Lucie Riu, Stephanie C. Werner

► To cite this version:

Jean-Christophe Viennet, Benjamin Bultel, Lucie Riu, Stephanie C. Werner. Diocahedral phyllosilicates versus zeolites and carbonates versus zeolites competitions as constraints to understanding early Mars alteration conditions. *Journal of Geophysical Research. Planets*, 2017, 122 (11), pp.2328-2343. 10.1002/2017JE005343 . hal-03127735

HAL Id: hal-03127735

<https://hal.science/hal-03127735>

Submitted on 10 Feb 2021

HAL is a multi-disciplinary open access archive for the deposit and dissemination of scientific research documents, whether they are published or not. The documents may come from teaching and research institutions in France or abroad, or from public or private research centers.

L'archive ouverte pluridisciplinaire **HAL**, est destinée au dépôt et à la diffusion de documents scientifiques de niveau recherche, publiés ou non, émanant des établissements d'enseignement et de recherche français ou étrangers, des laboratoires publics ou privés.

1 **Di octahedral phyllosilicates versus zeolites and carbonates versus zeolites**
2 **competitions as constraints to understanding early Mars alteration conditions**

3
4 Jean-Christophe Viennet^{a*}, Benjamin Bultel^{a*}, Lucie Riu^b, Stephanie C. Werner^a

5 ^a Centre for Earth Evolution and Dynamics, Department for Geosciences, University of
6 Oslo, Postboks 1028 Blindern, 0316 Oslo, Norway

7 ^b Institut d'Astrophysique Spatiale, Université Paris-Sud, 91400 Orsay, France

8 * Authors to whom correspondence should be addressed:

9 Jean-Christophe Viennet

10 Email address: j.c.viennet@geo.uio.no

Field Code Changed

11 Benjamin Bultel

12 Email address: benjamin.bultel@geo.uio.no

Field Code Changed

13 Centre for Earth Evolution and Dynamics, Department for Geosciences, University of
14 Oslo, Postboks 1028 Blindern, 0316 Oslo, Norway.

15

16 **Key points**

17 - Experiments and geochemical modeling to investigate the effect of CO₂ content on
18 mineral formation on ~~(early)~~ Mars.

19 - Dioctahedral phyllosilicates versus /zeolites and carbonates versus /zeolites formation as
20 a proxy to determining aqueous alteration history.

21 - Zeolite formation is inhibited in favor of carbonates by the presence of CO₂ in the
22 aqueous solution.

23 **Abstract**

24 Widespread occurrence of Fe,Mg-phyllsilicates have been observed ~~by remote sensing~~
25 ~~instruments~~ on Noachian Martian terrains. Therefore, the study of Fe,Mg-~~phyllsilicates~~smectite
26 formation, in order to characterize early Martian environmental conditions, is of particular
27 interest to the Martian community. Previous studies have shown that the investigation of Fe,Mg-
28 smectite formation alone helps to describe early Mars environmental conditions, but there are still
29 large uncertainties (in terms of pH range, oxic/anoxic conditions, etc.). Interestingly, carbonates
30 and/or zeolites have also been observed on Noachian surfaces in association with the Fe,Mg-
31 phyllsilicates.

32 ~~Drawing on this~~Consequently, the present study focuses on the di/tri-octahedral
33 phyllsilicate/carbonate/zeolite formation as a function of various CO₂ contents (100% N₂,
34 10% CO₂ / 90% N₂, 100% CO₂), from a combined approach including closed system laboratory
35 experiments for 3 weeks at 120°C and geochemical simulations. The experimental results show
36 that as the CO₂ content decreases, the amount of dioctahedral clay minerals decreases in favour
37 of trioctahedral minerals. Carbonates and dioctahedral clay minerals are formed during the
38 experiments with CO₂ and carbonates are formed ; while, when Ca-zeolites are formed, no
39 carbonates and dioctahedral minerals are observed. Geochemical simulation aided in establishing
40 pH as a key parameter in determining mineral formation patterns. Indeed, under acidic conditions
41 dioctahedral clay minerals and carbonate minerals are formed, while trioctahedral clay minerals
42 are formed in basic conditions with a the (neutral pH value of 5.98 at 120°C equal at). Zeolites are
43 favoured from pH >~7.2. The results obtained shed new light on the importance of dioctahedral
44 clay minerals ~~versus~~ zeolites ~~versus~~and carbonates versus /zeolites competitions, to better define
45 the aqueous alteration processes throughout e(early) Mars history.

Formatted: Not Superscript/ Subscript

46 **Keywords**

47 Mars, clay minerals, carbonates, zeolites, experiments, geochemical modeling

48 **1. Introduction**

49 Among the various hydrated minerals detected by remote sensing instruments (such as:
50 smectites (mainly Fe,Mg octahedral-rich), chlorites, kaolins, talc, serpentines and zeolites, in
51 decreasing order of occurrence [Carter *et al.*, 2013]), a particular interest has been devoted to the
52 study of Fe,Mg-smectites. Indeed, their discovery on the Martian surface is a crucial observation
53 because they could be an indicator for circum-neutral pH water activity, where a prebiotic
54 chemistry could have been developed during the early Noachian [Bibring *et al.*, 2006].

55 Hence, laboratory experiments [Dehouck *et al.*, 2016; Dehouck *et al.*, 2014; Peretyazhko
56 *et al.*, 2016] and/or geochemical simulation [Catalano, 2013; Chevrier *et al.*, 2007; Fernández-
57 Remolar *et al.*, 2011; Griffith and Shock, 1995; Liu and Catalano, 2016] have been devoted to
58 better understanding their formation. In particular, due to the Fe-rich Martian crust (compared to
59 the Earth's) and the current oxidizing conditions, redox effects on the formation of Fe,Mg-
60 smectites have been studied under conceivable early Martian environmental conditions. By using
61 geochemical modeling, Chevrier *et al.* [2007] suggest that the presence of nontronite (Fe³⁺-rich
62 smectite) could be the result of highly oxidizing conditions; while, Catalano [2013] argues for a
63 primary alteration period under reducing conditions followed by an oxidizing period, leading to
64 Fe³⁺-smectite formation. However, laboratory experiments [Dehouck *et al.*, 2016] have shown
65 that if early Mars had a dense CO₂ atmosphere, highly oxidizing conditions would have strongly
66 inhibited the formation of Fe,Mg-smectites and reducing conditions would have led to their
67 formation. Moreover, a circum-neutral pH is sufficient to obtain Fe,Mg-phyllsilicates from
68 volcanic rocks (especially basalt, Gysi and Stefánsson [2012a; 2012c]), but not necessarily.
69 Indeed, Peretyazhko *et al.* [2016] have experimentally demonstrated that the weathering of a
70 chemically representative Martian basaltic glass, with a water at pH 4 under oxic or anoxic N₂

71 atmosphere, leads to the formation of Fe,Mg-smectites. Finally, while our understanding of the
72 early Martian atmosphere is dependent on our understanding of Fe,Mg-phyllsilicates ~~(especially~~
73 ~~Fe,Mg-smectites)~~, their formation conditions are too wide to provide enough constraints for a
74 better understanding of the early history of Mars.

75 To a lesser extent, non-clay minerals associated with the Fe,Mg-phyllsilicates were
76 observed on the Noachian Martian surface, such as carbonates [Ehlmann *et al.*, 2008; Niles *et al.*,
77 2013; Wray *et al.*, 2016] and zeolites (Carter *et al.* [2013], see also section 2 of this paper). The
78 presence of carbonates could be linked to an early thicker CO₂-rich atmosphere [Morse and
79 Marion, 1999], which allows for the presence of liquid water (e.g., Pollack *et al.* [1987]). Brown
80 *et al.* [2010] propose that the formation of carbonates results from hydrothermal alteration of
81 basaltic rocks. The limits of carbonate formation in basaltic rocks on Earth has been investigated
82 in both experimental and modelling studies (e.g., CO₂ sequestration, [Gysi and Stefánsson, 2011;
83 2012a; b; c; Matter *et al.*, 2016]), but in Martian environments this is yet to be fully explored.
84 Indeed, geochemical simulation based on observations from altered Icelandic rocks ~~Icelandic~~
85 ~~observations~~ showed that hydrothermal alteration could be a source for carbonate formation and
86 that at least ~~one bar~~ 1 bar of pCO₂ could have been stored in the subsurface [Griffith and Shock,
87 1995]. The geochemical simulation of Chevrier *et al.* [2007] concluded that 1 bar of partial
88 pressure of CO₂ in oxidizing conditions could inhibit the formation of carbonates ~~(while Fe,Mg-~~
89 ~~smectites will be formed)~~. On the other hand, the experimental work of Dehouck *et al.* [2016]
90 showed that the formation of carbonates is possibly enhanced by highly oxidizing conditions
91 under a dense CO₂ atmosphere (from 0.8 up to 1.5 bars). Therefore, it is suggested that
92 atmospheric conditions could have a strong influence on the formation of carbonates and/or
93 Fe,Mg-phyllsilicates, and could be used as a probe to better understand the early Martian

94 environment. In addition to carbonates, zeolite formation and stability are strongly dependent on
95 the geochemical conditions (such as alkaline pH solution, [Dyer, 2002]), and are therefore a good
96 probe to investigate the Martian environmental conditions [Ming and Gooding, 1988]. Like clay
97 minerals, zeolites are of prime importance, because they have a high potential for being major
98 sinks of atmospheric gas [Ming and Gooding, 1988; Mousis et al., 2016]. They can sorb and
99 protect organic compounds and act as a catalyst for organic-based reactions [Ming and Gooding,
100 1988; van Bekkum and Kouwenhoven, 1989; Venuto, 1994]. Although, zeolite formation in
101 Martian environments has not been widely studied, links between carbonation and clay formation
102 (mainly smectite) from basaltic rocks has already been observed in hydrothermal (natural and
103 laboratory simulated) systems on Earth [Dyer, 2002; Gysi and Stefánsson, 2012a; c; Kralj et al.,
104 2010; Stefánsson and Gíslason, 2001; Utada, 1988].

105 A review of zeolites detected on Noachian terrains is given in section 2, highlighting the
106 associated minerals and probable geological processes. The aim of the present study is to
107 investigate the formation of phyllosilicates/carbonates/zeolites by experimental work, in closed
108 systems with various aqueous CO₂ levels (100% N₂, 10% CO₂ / 90% N₂, 100% CO₂). Note that
109 due to the use of closed systems, the purpose of this study is not an attempt at determining pCO₂
110 level(s) of the Martian atmosphere. The cause and source of various aqueous CO₂ levels could be
111 driven by either atmospheric and/or magmatic interaction [as explained in Brown et al., 2010;
112 Bultel et al., 2015]. The various CO₂ % are chosen to reflect 1 order of magnitude of CO₂ content
113 between each experiment. To better define this behaviour, we report on geochemical simulations
114 constrained by the experimental results. Finally, the results obtained are used to evaluate better
115 determine the environmental conditions during the early Noachian epoch. Compared to the sole
116 investigation of clay minerals, shed new light on the importance of di/tri-

Formatted: Subscript

117 ~~phyllosilicate/carbonate/zeolite formation~~ dioctahedral clay minerals versus zeolites and
118 carbonates versus zeolites competitions is used during the early Noachian epoch and to highlight
119 the pH conditions during the alteration ~~will help to better determine the environmental conditions~~
120 ~~for such alteration products.~~

2. Martian Zeolites

2.1 Remote sensing detection of zeolites

In the near-infrared domain, ~~sampled by instruments in orbit around Mars, zeolites have~~
~~specific absorption bands near 1.20, 1.40, 1.90, 2.70-3.10 μm and one centered at 2.40-2.50 μm .~~
~~The latter is attributed to the cation-OH liaison while the others are attributed to structural water~~
~~or absorbed water on its surface. zeolites have specific absorption bands near 1.20, 1.40, 1.90,~~
~~2.70-3.10 μm , attributed to structural water or absorbed water on its surface, and at 2.40-2.50 μm ,~~
~~attributed to the cation-OH liaison~~ [Cloutis et al., 2002]. The detection of zeolites on the Martian
surface is usually confirmed by a combination of absorptions near 1.40 and 1.90 μm due to
hydration, and reduced reflectance from 2.30 μm due to a large absorption centered near
2.50 μm . Except for analcime identified by its specific NIR feature ~~a (band near 1.79 μm)~~,
identification of other types of zeolites is challenging when mixed with hydrated minerals such as
phyllosilicates. Indeed, the absorptions near 1.40 and 1.90 μm are common spectral bands among
hydrated minerals. Therefore, no specific absorption can be attributed to zeolite if mixed with
other hydrated minerals. However, the “zeolite background” spectrum is specific and, hence,
zeolite detection is possible from the inflexion band after 2.30 μm . In addition to phyllosilicates,
sulfates have a similar spectral shape ~~with (bands near 1.90 and 2.50 μm)~~. In this particular case,
the geological context could be used as criteria to characterize the mineralogy. For example, the
detection by proximity of monohydrated sulfates, kaolin, opal and nontronite suggest acidic
environment, which is more favorable for sulfate than zeolite formation, as explained in Pajola et
al. [2016].

Formatted: English (United States)

142

2.2 Absence and controversial detection of zeolites

143 Unlike the main alteration products—observed on the Martian surface [such as \(i.e. Fe,Mg](#)
144 [clay minerals, carbonates, etc...\)](#), zeolites have not been reported in Martian meteorites (*Gooding*
145 [1992]; *Tomkinson et al.* [2013]). Nevertheless, Martian meteorites may not be representatives of
146 the main Martian alteration features [*McSween*, 1994]; therefore, the zeolite formation process
147 cannot be understood from meteorites. *Ruff* [2004] suggests that zeolite is a component of the
148 dust on Mars from thermal infrared data. It could be an indication of a widespread zeolite
149 presence on the Martian surface. Nevertheless, the zeolite presence in Martian dust is uncertain
150 and disputed [*Bandfield et al.*, 2003]. Zeolites [mixed with hydrated silica, opaline](#) have also been
151 suggested in the faulted region of Nili Fossae [*Ehlmann et al.*, 2009; *Viviano et al.*, 2013], and at
152 the bottom of stratigraphic profiles in Terby crater and Eridania Basin, [with a sequence](#) (from top
153 to bottom: [of Al-phylosilicates, Fe,Mg-phylosilicates and possibly zeolite with hydrated silica](#)
154 [\(opaline\)](#); [*Ansan et al.* [2011](#)]; *Carter et al.* [2015](#)]; *Carter et al.* [2010](#)]; *Carter et al.* [2013](#)];
155 *Pajola et al.* [2016](#)]). However, these detections remain uncertain because identification is based
156 on the shape of [spectra near 2.5 µm observed by](#) the ~~CRISM~~ (Compact Reconnaissance Infrared
157 Spectrometer for Mars ~~(CRISM)~~ [spectra near 2.5 µm](#).

158

2.3 Reliable zeolite detections

159 Zeolites have been detected on crustal outcrops via [CRISM Compact Reconnaissance](#)
160 [Imaging Spectrometer for Mars \(CRISM\)](#) ~~CRISM~~ data [*Ehlmann et al.*, 2011; *Sun and Milliken*,
161 2015; *Viviano-Beck et al.*, 2017; *Wray et al.*, 2009] together with Fe,Mg-rich phyllosilicates,
162 hydrated silica or carbonates. We can now classify the different detections of zeolite by mineral
163 associations. It is possible to distinguish three classes of zeolites based on their association with
164 (i) Fe,Mg-phylosilicates (Fe,Mg-smectites and/or chlorites) and hydrated silica; (ii) Fe,Mg-

Formatted: English (United Kingdom)

Formatted: French (France)

165 phyllosilicates (~~Fe,Mg-smectites and/or chlorites~~) and carbonates; and (iii) only Fe,Mg-phyllosilicates (~~Fe,Mg-smectites and/or chlorites~~).

166 Near Nili Fossae, few craters excavated an association of ~~zeolite (analcime)~~, Fe,Mg-
167 phyllosilicates (mainly chlorite and possible prehnite) and hydrated silica [Ehlmann *et al.*, 2011].

168 The association of zeolites with Fe,Mg-phyllosilicates and carbonates is found in Valles
169 Marineris (see Viviano-Beck *et al.* [2017]). Zeolites in association with only Fe,Mg-smectites
170 and/or chlorite are found in impact craters or in valleys formed by tectonic activity [Viviano-Beck
171 *et al.*, 2017]. No particular stratigraphy is related to these detections. Moreover, detections are
172 concentrated on ~~the~~ spurs (lateral ridge on the wall of a valley) or on the re-entrant (terrain
173 between two spurs) of the canyon [Ehlmann *et al.*, 2009; Loizeau *et al.*, 2012; Sun and Milliken,
174 2015; Viviano-Beck *et al.*, 2017; Viviano *et al.*, 2013]. In at least three craters where zeolite is
175 found with Fe,Mg-phyllosilicates, few authors suggest that a possible prehnite detection could be
176 present [Ehlmann *et al.*, 2009; Sun and Milliken, 2015; Viviano *et al.*, 2013].

177 The detection of zeolites on Mars on crustal outcrops is therefore always associated with
178 Fe,Mg-phyllosilicates (~~smectite and/or chlorite~~) and, in a few instances, with carbonates or
179 hydrated silica. Note that, when analcime has been detected, no other zeolite types have been
180 found nearby.

181 2.4 Possible process of formation

182 In cases of co-detection of zeolites, Fe,Mg-phyllosilicates and hydrated silica, the latter is
183 found only on crater floors, while zeolites and phyllosilicates are found in both crater floors and
184 the central structure. Their location could suggest post-impact hydrothermalism. Moreover, their
185 detection in the ejecta layer, which would imply an alteration before the impact, is missing. In the
186 case of zeolite detections exposed in the walls of Valles Marineris (assemblages ii and iii, see

187 section 2.4), they do not represent a particular stratigraphy [Viviano-Beck *et al.*, 2017]. The
188 authors suggest hydrothermal alteration of layers in the subsurface prior to the opening of the
189 canyon. The presence of zeolites in impact craters together with Fe,Mg-phyllsilicates (with or
190 without carbonates), are attributed to either hydrothermalism before or after the impact, or
191 diagenesis [Viviano-Beck *et al.*, 2017; Ehlmann *et al.*, 2009; Sun and Milliken, 2015]. However,
192 the possibility of burial diagenesis seems unlikely since detection of the zeolite zonation (i.e.
193 analcime to mordenite/clinoptilolite transformation) in the stratigraphy is lacking [Hay and
194 Sheppard, 2001]. On the other hand, the zonation could also be below the resolution and the
195 detectability of the instrument. Without a clear stratigraphic sequence unambiguously revealing
196 zeolites, diagenesis, as well as surface weathering, are unlikely the source of zeolite formation on
197 Mars. The most probable geological process resulting in the majority of zeolite detections could
198 be hydrothermal systems, from ambient temperature to <200°C when prehnite is not present. This
199 is in good agreement with the preferred alteration processes proposed for the alteration of the
200 Noachian crust [Carter *et al.*, 2013].

201 Based on these surveys dedicated to zeolites and to the processes of formation of
202 phyllosilicates and/or carbonates on Martian surfaces (see introduction), hydrothermal
203 experiments have been set up to reproduce the main mineralogical assemblages described above
204 (Fe,Mg-phyllsilicates/carbonates, Fe,Mg-phyllsilicates/zeolites). To do so, we set up closed
205 system laboratory experiments for 3 weeks at 120°C with different percentages of CO₂ to study
206 the aqueous alteration of basaltic glass, ~~and use g~~Geochemical simulations are used to decipher
207 the pH conditions, ~~especially water pH~~, controlling the minerals formation ~~of minerals~~.

208 3. Materials & Methods

209 3.1 Starting material and sample preparation

210 The raw material used for this study is a volcanic basaltic glass of tholeiitic composition
211 from Iceland (Stapafell, Reykjanes Peninsula). The pristine rocks were manually crushed and the
212 fraction between 0.5 to 1 mm was collected by using sieves. The 0.5-1 mm size fraction was
213 cleaned by washing the particles with deionized water in an ultrasonic bath. Then, the particles
214 were immersed in hydrochloric solution at pH 3 for 1 hour to remove any possible carbonates and
215 washed three times in distilled water. The millimetric particles were manually crushed in a mortar
216 to decrease the particle size to sizes between 100 and 500 μm . Finally, the particle size ~~(of less~~
217 ~~than 10 μm)~~ used for the experiments was obtained by crushing the 100-500 μm size fractions
218 using a micro-mill to obtain particles < 10 μm . The total chemistry of the final product was
219 obtained by fusion and XRF analysis (Actlabs, Canada, Table 1). The chemical composition of
220 the basaltic glass is in the range of the chemical composition range of Noachian Martian
221 meteorites [Agee *et al.*, 2013; Lodders, 1998], orbital [Boynton *et al.*, 2007] and in-situ analysis
222 [Gellert *et al.*, 2006; McSween *et al.*, 2009; McSween *et al.*, 2006; Ming *et al.*, 2008] performed
223 on the Martian surfaces.

224 3.2 Experimental set-up and procedure

225 The hydrothermal experiments were performed in closed systems at 120°C for a duration
226 of 3 weeks in a 600 mL Parr Reactor ©. 4.0 g of the <10 μm size fraction was mixed with 80 ml
227 of pure water and filled to the Parr reactor container leading to a gas head space of 520 ml at
228 room temperature. The pure-water and head_space were flushed for 10 minutes by injection of the
229 desired gas into the reactors through two valves. Then the reactors were sealed and heated to
230 120°C. Three different high purity gases were used for the experiments: Nitrogen (100% N₂),
231 Carbon Dioxide (100% CO₂) and a mixture of 10% CO₂ and 90% N₂, referred to as 10% CO₂ /

232 90% N₂ (with a CO₂ content uncertainty of less than ±1%). Note that, the experiments are
233 referred to by the percentage of the initial content of CO₂ and/or N₂.

234 **3.3 Solid phase analysis**

235 *3.3.1 X-Ray diffraction analysis*

236 On the bulk and altered rocks, X-Ray diffraction (XRD) patterns were recorded with a D8
237 Advance Bruker (CuKα₁₊₂ radiations) from 2 to 55°2θ using a step interval of 0.25°2θ and a
238 counting time per step of 2.5 s. The size of the divergence slit, the two Soller slits and the
239 antiscatter slit were 0.25°, 2.5°, 2.5° and 0.5°, respectively. The bulk initial and final materials
240 were analyzed on powder preparation. The clay minerals were analyzed by performing Ca- and
241 K-saturation using four saturation cycles with 0.5 mol.L⁻¹ of CaCl₂ and 1 mol.L⁻¹ of KCl,
242 respectively. Then the solutions were washed in distilled water and dried at 50°C. The XRD
243 patterns for clay minerals were recorded from oriented samples, prepared by pipetting slurries of
244 the particles dispersed in distilled water on glass slides and drying these at room temperature. The
245 Ca- preparations were analyzed after air-dried preparation (the associated acronym is Ca-AD).
246 Thereafter, the glass slides were exposed to ethylene-glycol vapor at 50°C overnight to obtain
247 ethylene-glycol solvation; the subsequent XRD patterns recorded are referred to as Ca-EG. Heat
248 treatments at 110°C, 330°C and 550°C were performed on the K-saturated glass slide
249 preparations and the respective XRD patterns were recorded (referred to as K-110, K-330 and K-
250 550, respectively). To obtain these XRD patterns for the different treatments, the slides were
251 progressively heated over 4 hours stopping at each specific temperature to allow the slides to cool
252 down to ambient temperature before XRD analysis was acquired.

253 3.3.2 Near Infra-red analysis

254 The near-infrared reflectance spectra were obtained with a PerkinElmer FTIR
255 spectrometer. The wavelength range explored is from 1 to 4 μm with a spectral resolution of 1
256 cm^{-1} and a spectral sampling of 0.4 nm. On the bulk and altered rocks, the reflectance spectra
257 were acquired on rock powder preparation under ambient temperature and pressure conditions.
258 Additionally, a calibration was carried out prior to the analysis to derive the samples reflectance
259 spectra, using an *Infragold* and a *Spectralon* 99% sample from Labsphere.

260 3.4 Geochemical simulation

261 The aim of the geochemical simulation exercise is to reproduce the mineralogical
262 association obtained during the experiments as a function of the initial gas composition for the
263 same rock composition, temperature and water/rock ratio. The thermodynamic simulations were
264 performed by using the EQ3/6, software version 8.0 [Wolery, 1992a; b; Wolery *et al.*, 1990].

265 Backward reactions are authorized ~~(e.g. which means that the dissolution of the product is~~
266 ~~authorized)~~. The thermodem data base (<http://thermoddem.brgm.fr/>) was used to account for
267 updated clay minerals and zeolite thermodynamic values compared to the *data0.cmp* database

268 ~~(see Table 2), (e.g., Fe rich saponite (1 Fe atom in substitution of 1 Mg atom in the octahedral~~
269 ~~sheet), sudoite, sudoite(Fe), vermiculite, illite, phillipsite, clinoptilolite, heulandite, chabazite,~~
270 ~~mordenite and stellerite). Ideal solid solutions were used during the geochemical exercise~~
271 ~~with the following structural formula: $\text{Si}_1\text{Al}_{0.35}\text{Fe}_{0.23}\text{Mg}_{0.29}\text{Ca}_{0.26}\text{K}_{0.07}\text{Na}_{0.01}\text{O}_{3.345}$ was~~

272 The basaltic glass used during the experiments was also implemented in the database. The
273 following structural formula of the basaltic glass $\text{Si}_1\text{Al}_{0.35}\text{Fe}_{0.23}\text{Mg}_{0.29}\text{Ca}_{0.26}\text{K}_{0.07}\text{Na}_{0.01}\text{O}_{3.345}$ was
274 calculated from the total chemistry (Table 1) and it is ~~similar to~~ in accordance with previous
275 studies using similar volcanic glass [Aradóttir *et al.*, 2012; Gysi and Stefánsson, 2011]. The

Field Code Changed

276 estimation of the $\log(K)$ values for the dissolution of the basaltic glass were based on a
277 theoretical approach [Paul, 1977], which considers the glass as oxide mixtures. Then, the
278 solubility of the volcanic glass corresponds to the sum of the solubility products of the oxides
279 weighted by the mole fractions. The values obtained (Table 1) are in good agreement with
280 previous data on similar Icelandic volcanic glass [Aradóttir et al., 2012].

281 To mimic the experimental procedure, we first saturate the water with the desired
282 atmosphere. ~~Therefore, we~~ We put in contact ~~80 grams (80 mL)~~ of pure water with the desired gas
283 at 25°C and at atmospheric pressure. ~~The~~ number of mol of gas was calculated by considering
284 the volume of the head space in the reactor. Then, the aqueous solution and the atmosphere are
285 heated in a closed system model until the experiment's nominal temperature (120°C) is reached.
286 ~~Therefore~~ Hence, the total content of C ~~(for the experiments involving CO_{2(g)})~~ in the system is
287 constant and similar to the experimental value. The last step of the geochemical simulation
288 consists of mixing ~~the~~ 4 grams of basalt with the gas/water components and then letting the
289 simulation reach equilibrium as a function of the mol of basalt destroyed (% of dissolution).

290 The numerical setup is slightly different compared with the experimental procedure. The
291 original basalt is put in contact with the aqueous solution at 120°C during the simulation while
292 ~~For the exper~~ during the experiments the original basalt is mixed with pure water at 25°C and then
293 heated ~~to~~ 120°C. However, ~~this difference does not alter the simulated results compare to the~~
294 experimental ones. ~~The~~ slow reaction of basalt ~~at this temperature,~~ compared with the 1 hour
295 heating time ~~(less than 1 hour)~~ required to reach 120°C during the experiments, likely prevents
296 alteration and minerals ~~formation formation and no stable thermodynamical state can be reached~~
297 during this period. The geochemical simulations take in account all ~~the~~ minerals present in the
298 data base even if they are not in equilibrium in such pressure and temperature conditions. Hence,

299 ~~In comparison, preliminary during the geochemical simulations were performed. Then, minerals which are not assumed to~~
300 ~~form in such systems/environments/conditions, are suppressed (see table 2). The final geochemical simulations~~
301 ~~corresponds to minerals formation possible in such temperature and pressure range.. Thus,~~
302 ~~although given in the database, minerals are suppressed if formed in much higher temperature~~
303 ~~and/or pressure ranges (e.g., prehnite, olivine, magnetite, biotite, graphite, wollastonite,~~
304 ~~amphibole and epidote) and in metamorphosed sediments (e.g., akermanite, monticellite and~~
305 ~~merwinite), as well as in lower temperature ranges (e.g., chabazite [Blanc, 2009]). In addition, the~~
306 ~~minerals which are already taken into account in the solid solution products are also suppressed,~~
307 ~~such as, dolomite, dolomite ordered and disordered (carbonates solid solution from calcite,~~
308 ~~magnesian dolomite (calcite solid solution). Finally, the spinel has been considered, but it is not actually formed in a brine~~

309 **4. Results**

310 **4.1 Experimental results**

311 The figure 1.I and 1.II presents the XRD powder patterns and the NIR spectra obtained on
312 the unreacted sample (a) and after the experiments as a function of the gas composition (b, c and
313 d under 100% CO₂, 10% CO₂ / 90% N₂ and 100% N₂, respectively). The large and intense bump
314 between 5 and 2.33 Å, centered at 3.23 Å of the unreacted sample (Figure 1.I.a and 1.II.b) defines
315 is composed mainly of a volcanic glass. The triangles at 5.12, 3.89, 3.50, 2.78, 2.52, 2.47,
316 2.36, 2.27, 2.56, 2.17 and 1.75 Å (Figure 1.I.a, large and intense bump between 5 and 2.33 Å,
317 centered at 3.23 Å) with a correspond to a small proportion of forsterite (Figure 1.I.a, triangles at
318 5.12, 3.89, 3.50, 2.78, 2.52, 2.47, 2.36, 2.27, 2.56, 2.17 and 1.75 Å), the stars at 4.26 and 3.33 Å
319 correspond to quartz (Figure 1.I.a, stars at 4.26 and 3.33 Å) and the diamonds at 3.20 and 2.99 Å
320 correspond to a minor amount of pyroxene (Figure 1.I.a, diamonds at 3.20 and 2.99 Å). The
321 volcanic glass and quartz minerals have no specific absorption bands in this NIR range, which
322 lead to a high intensity band corresponding to olivine and low-calcium pyroxene (LCP)
323 (Figure 1.II.a, at 1.07 and 1.85 μm, respectively) [*Hunt and Salisbury, 1970*]. The large spectral
324 band at around 2.90 μm corresponds to H₂O molecules present in the sample probably adsorbed
325 on the edges of the basaltic particles (Figure 1.II.a). All XRD patterns obtained on the reacted
326 materials show a decrease in the broad peak intensity (Figure 1.I.b, c and d) corresponding to the
327 volcanic glass (Figures 1.I.a). These intensity decreases indicate that the initial glass was
328 dissolved and that minerals were formed during the experiments (Figure 1.I). ~~(corresponding to~~
329 ~~the appearance of XRD peaks indexed by their position in Å on the XRD patterns, figure 1.I, and~~
330 ~~the indexed spectral band in μm, figure 1.II).~~To assess the rate of dissolution % of the volcanic
331 glass, the full pattern fitting method [*Chipera and Bish, 2013*] was applied. This method consists
332 of determining the difference in area between the XRD peaks corresponding to both the original

333 glass and the weathered sample. The results obtained show that 19, 23 and 25% of volcanic glass
334 ($\pm 2\%$, uncertainty on laboratory mixture between basaltic glass and zinc) was dissolved during
335 the experiments under 100% N₂, 10% CO₂ / 90% N₂ and 100% CO₂ initial gas mixtures,
336 respectively. The intensities of the XRD peaks corresponding to forsterite, pyroxene and quartz
337 do not display ~~any~~ differences between the unreacted basalt and all the weathered products. This
338 means that they have not been ~~weathered~~ dissolved completely during the
339 experiments.

340 For non-clay minerals, the XRD peaks at 3.02, 2.48 and 1.87 Å (Figure 1.I.b) indicate the
341 presence of Ca-Mg-Fe carbonate for the 100% CO₂ experiment while for the 10% CO₂ / 90% N₂
342 experiment, the XRD peaks at 3.85, 3.04, 2.49, 2.09, 1.93, 1.91 and 1.88 Å (Figure 1.I.c)
343 correspond to calcite. The NIR spectra confirm the presence of carbonates, due to the spectral
344 band at 3.85 and 3.98 μm corresponding to the C-O liaison (Figure 1.II.b and c, [Gaffey, 1985
345 and Hunt, 1977]). Note that, during the 100% N₂ experiment no carbonate mineral was formed.
346 The XRD peaks at 7.13, 4.94, 4.14, 4.06, 3.25, 3.13 and 2.67 Å correspond to the formation of
347 garronite zeolite for the experiment under 100% N₂ (Figure 1.I.d), while no zeolite is formed in
348 experiments involving CO₂ gas (Figure 1.I.b and c). There is no evidence of a characteristic
349 zeolite band from the NIR analysis. This could either be due to low proportions relative to the
350 trioctahedral phyllosilicates, and/or due to overlapping of the characteristic spectral bands for
351 phyllosilicates and zeolites. Indeed, the bands near 1.41 μm and at 1.91 μm correspond to the
352 bending and stretching overtone of bound water, and between 2.19 - 2.5 μm to cation-OH liaison
353 (Figures 1.II.b, c and d). The combination of bands at 2.76, 2.90 and 3.07 μm (Figures 1.II.b, c
354 and d) corresponds to OH fundamental stretching and H₂O stretching in di/tri-octahedral

355 phyllosilicates, such as, smectites and/or chlorites [Bishop *et al.*, 1994; Clark *et al.*, 1990; Hunt
356 and Salisbury, 1970].

357 The presence of clay minerals can be confirmed by the bulk XRD patterns due to the
358 presence of 00*l* reflections at 15.09 and 2.57 Å (Figures 1.I.d c and b), at 7.35 and 2.39Å under
359 10% CO₂ / 90% N₂ and 100% CO₂ experiments (Figures 1.I.b and c, respectively); as well as
360 020 reflections at 4.57 Å (Figures 1.I.b, c and d). No evidence of rational series of 00*l* reflections
361 (*l*×00*l* is constant for all the reflections) was seen; therefore, clay minerals present in the samples
362 are mainly mixed layer minerals (MLM). More detailed identification of clay minerals present in
363 the samples after the experiments, was performed using conventional XRD treatments (See
364 section 3.3.1 and Figures 2.I and II) and by removing the continuum of the spectral data to
365 highlight the absorption band intensities (Figure 2.III). The determination of the di/tri-octahedral
366 characters of the minerals formed are based on the NIR analysis and not on the XRD patterns
367 dedicated to the d(060) peaks (see supplementary Figure S1). Indeed, the XRD patterns dedicated
368 to the measurement of the d(060) (Figure S1) exhibit only slight differences in peak position
369 between the three experiments. Conversely, the NIR analysis (Figure 2.II) exhibits more variation
370 on the di/tri-octahedral character of the minerals formed. Different reasons can be evoked, as
371 explained below. The NIR analysis is a direct probe to investigate the metal-OH bond in the
372 octahedral sheet of clay minerals (see Petit and Madejova, [2013] and references therein).
373 Therefore, NIR analysis is less affected by the difference in poorly compared to well crystalline
374 clay minerals formed than XRD analysis, and in addition NIR spectroscopy has already been
375 largely used in the identification of di/tri-octahedral clay minerals on the Martian surface (See
376 Carter *et al.*, [2015] and references therein). Moreover, the investigation of the di/tri-octahedral
377 clay minerals via the d(060) position could be more difficult than explained by Brindley and

378 *Brown*, [1985]. In fact, the d(060) peak position is also dependent on the amount of Fe³⁺/Al³⁺
379 substitution in the octahedral and/or tetrahedral sheets [*Baron et al.*, 2017; *Iriartre et al.*,2005;
380 *Petit and Decarreau*, 1990; *Petit et al.*, 2015]. Depending on the Fe³⁺/Al³⁺ content (~~both~~
381 octahedral and/or tetrahedral), the d(060) could reflect the position of trioctahedral clay minerals
382 (~1.54 Å, *Brindley and Brown*, [1985]), while only dioctahedral clay minerals are present [*Petit*
383 *et al.*, 2015]. ~~NIR analysis is also less affected by the difference in crystallinity of the clay~~
384 ~~minerals formed than XRD analysis.~~ Additionally, non-clay minerals calcite, forsterite and quartz
385 present XRD peaks in the range of the 060 peaks analysis, complicating interpretation.

386 For the 100% N₂ experiment (Figure 2.I.c, 2.II.c), the reflection at 14.82 Å in the Ca-AD
387 state shifts to 16.69 Å, and its 002 reflection at 8.35 Å appears in the Ca-EG state. Moreover, the
388 reflection shifts to 11.55 Å in the K-110 state and then to 10.41 Å after heating at 330 and 550°C.
389 This XRD behavior is attributed to smectite layers. NIR confirmed this analysis with V-shaped
390 bands at 1.91 and 2.31 μm (Figure 2.III.c), which correspond to H₂O stretching and bending
391 bands, and (Fe,Mg)₃-OH stretching and bending bands of trioctahedral smectite, respectively.
392 The absorption band at 2.35 μm could correspond to (Fe,Mg)₃-OH liaisons of Fe-rich
393 trioctahedral chlorite (Figures 2.III.a, b and c) [*Bishop et al.*, 2008; *King and Clark.*, 1989]. The
394 band near 2.43 μm (Figures 2.III.b and c) could be due to the presence of Fe²⁺ and/or Mg²⁺ in the
395 octahedral sheet of TOT phyllosilicates and its intensity is related to the relative amount of Fe
396 and Mg [*Mustard*, 1992]. The position and the strength of this band would indicate a high Fe
397 content in the smectite layers for the 100% N₂ experiment. The slight band at 2.25 μm (Figures
398 2.III.a and b) corresponds to Al³⁺,Fe³⁺-OH bending and stretching overtone in dioctahedral
399 chlorite and/or smectite. Therefore, from the XRD behavior and NIR analysis, this sample

400 ~~constitutes is composed of a trioctahedral-rich smectite and to a lesser extent of a minor proportion of a dioctahedral smectite or~~
401 ~~chlorite mixed-layer mineral (MLM).~~

402 With CO₂ % increase (Figures 2.I.b, 2.I.a, 2.II.b, 2.II.a, 2.III.b, 2.III.a), the XRD behavior
403 of smectite layers ~~corresponding to a~~ (shift of the XRD peaks between Ca-AD and Ca-EG state to
404 lower angles) becomes less pronounced and spectral band intensities of the smectite layers
405 decreases. ~~The~~ absorption of the hydration band near 1.9 μm, ~~the absorption band of~~ (Fe,Mg)₃-
406 OH liaison at 2.31 μm ~~decrease and the band at 2.43 μm disappearance disappears of the band at~~
407 ~~2.43 μm,~~ (Figures 2.III.a and b). While this phenomenon could be partly attributed to a decrease
408 in the coherent scattering domain size of the clay minerals, it mainly indicates a decrease in
409 trioctahedral smectite layers content with the CO₂ % increase. Inversely, the XRD peak
410 intensities at 7.35 Å in the Ca-AD state increase with the CO₂ % (Figures 2.I.a, b). This XRD
411 peaks shifts slightly to 7.60 Å in the Ca-EG state and hence shows the presence of smectite layers
412 (Figures 2.I.a and b). Moreover, this XRD peak does not shift between 110 - 330°C and
413 disappears after 550°C (Figures 2.II.a and b). This XRD behavior is suggestive of kaolinite layers
414 and/or of the 002 reflection of Fe-rich chlorite layers (dehydration of the octahedral sheet of 2:1
415 layer of Fe(II) rich chlorite below 550°C; *Barnishel and Bertsch*, [1989]). However, the infra-red
416 spectra do not exhibit the characteristic bands of kaolinite (at 2.16 and 2.2 μm, *Bishop et al.*,
417 [2008]); ~~In addition, therefore, no kaolinite layers are present in these samples. T~~he absorption
418 bands at 2.35 μm are more pronounced with the CO₂ % increase and disappear after heating at
419 550°C (See supplementary Figure S2). This band could be linked to (Fe,Mg)₃-OH liaisons of
420 Fe-rich trioctahedral chlorite [*King and Clark.*, 1989]. Note that, this XRD and NIR behavior
421 could not be attributed to serpentine (while the XRD peak position could correspond to
422 serpentine) because its dehydration temperature is at 600°C [*Dlugogorski. and Balucan*, 2014].

423 Therefore, from the XRD behavior and the 2.35- μm NIR band analysis, this clay mineral constitutes is mainly a Fe-rich
424 dioctahedral MLM with a minor content of Fe-rich trioctahedral MLM in the Fe-rich MLM in the Fe-rich MLM
425 compared to the trioctahedral smectite, content for the 100% N₂ experiment, increases with the CO₂%. In addition with the CO₂%
426 increase, the dioctahedral character of the clay minerals is increasingly pronounced and can be
427 assessed by the NIR analysis. The due to the intensity intensities increase of the 2.19 and 2.25 μm spectral band (Figures
428 2.III.a, b and c), which are related to Al₂-OH and (Al,Fe)₂-OH liaison, increase with the CO₂ %.
429 These bands correspond to dioctahedral smectite/chlorite MLM. The presence of this MLM is
430 confirmed by XRD due to the shift of the peak positions at 14.82 and 16.69 Å in the Ca-AD and
431 CA-EG state, respectively (Figures 2.I.a, b and c).

432 Table 32 presents the summary of minerals formed during the experiments. The results
433 obtained show that zeolites formed without carbonate formation for the 100% N₂ experiment,
434 while carbonates without zeolites are formed under experiments involving CO₂. Moreover, with
435 the increase in CO₂ levels, the trioctahedral smectite/chlorite MLM content decreases, while the
436 dioctahedral MLM increases. In addition with the increasing CO₂ levels, the relative content of
437 trioctahedral smectite layers decreases relative to in favor of the Fe-rich trioctahedral chlorite,
438 with increasing CO₂ levels. Note that, zeolite mineral formation during the 100% N₂ experiment
439 cannot be observed by NIR analysis, but XRD analyses confirms its presence.

440 4.2 Geochemical model results

441 To better understand the mechanism leading to mineral formation as a function of gas
442 composition, geochemical modeling was performed and constrained by the experimental results
443 (for more details see section 3.4, materials and methods).

444 At first~~In a first time~~, the geochemical simulations are run until the given dissolution
445 basaltic glass % estimated by XRD is reached. This solution has been chosen rather than a

Formatted: Subscript

446 kinetics method in order to avoid any limitation due to clay minerals, carbonates and zeolites
447 formation, which lead to a decrease of the dissolution rate of the basaltic glass (see for example,
448 Stockmann et al. [2008]). Then, The results obtained from the geochemical modeling are
449 presented at the corresponding percentage of glass dissolution determined by XRD for each
450 experiment (see section 4.1) results and are compared to the mineral identification results (Table
451 32). The aim is to compare mineral formation between the experimental results and the
452 geochemical simulation, in order to confirm that the results obtained by the geochemical
453 simulations are coherent with the experiments. The clay minerals identification has shown that
454 their crystal structure constitutes sa-stacking of layers with different nature* (mixed-layer-
455 minerals). Nevertheless, the geochemical simulation does not take into account the formation of
456 these MLMs. Indeed, even if solid-solution products ((same layer nature but different interlayer
457 cations)) are authorized, it does not simulate mixed-layer minerals. Therefore, clay mineral
458 identification (Table 2 and 32) is split into two families, the di- and tri-octahedral phyllosilicates.
459 The dioctahedral phyllosilicates formed during the simulations consist of the sum of
460 montmorillonite (mainly $(\text{Mg,Ca})_{0.165}\text{Mg}_{0.337}\text{Al}_{1.67}\text{Si}_4\text{O}_{10}(\text{OH})_2$), nontronite (mainly
461 $(\text{Mg,Ca})_{0.165}\text{Fe}_2\text{Al}_{0.33}\text{Si}_{3.67}\text{O}_{10}(\text{OH})_2$), dioctahedral chlorite $(\text{Fe,Mg})_2\text{Al}_4\text{Si}_3\text{O}_{10}(\text{OH})_8$ and kaolinite
462 $(\text{Al}_2\text{Si}_2\text{O}_5(\text{OH})_4$). The trioctahedral phyllosilicates formed during the simulations correspond to
463 the sum of saponite (mainly $(\text{Mg,Ca})_{0.165}\text{Mg}_3\text{Al}_{0.33}\text{Si}_{3.67}\text{O}_{10}(\text{OH})_2$), trioctahedral chlorite
464 $(\text{Fe,Mg})_3\text{Al}_2\text{Si}_4\text{O}_{10}(\text{OH})_8$ and talc $(\text{Fe,Si}_4\text{O}_{10}(\text{OH})_2$). Due to the lack of garronite in the geochemical database, the zeolites considered and
465 that appear during the geochemical simulation are mainly gismondine $(\text{Ca}_2\text{Al}_3\text{Si}_4\text{O}_{16}\cdot 9\text{H}_2\text{O})$ and, to a lesser extent,
466 phillipsite $(\text{Na,Ca}_{0.5})_4\text{Al}_5\text{Si}_8\text{O}_{38}\cdot 3\text{H}_2\text{O}$. Gismondine, phillipsite and garronite belong to the group of zeolites with chains of
467 edge-sharing four-membered rings [Dyer, 2002]. In particular the gismondine, which is the
468 zeolite mainly formed during the geochemical simulation, has the same subgroup structure type
469 as the garronite: the GIS group. Moreover, the structural formula of garronite

Formatted: Font: Italic

470 (Ca_{2.5}NaAl₆Si₁₀O₃₂·13H₂O) is similar to that of gismondine and phillipsite zeolites (in terms of
471 cation content). In addition, the Si/Al ratio of garronite is comprised between the Si/Al ratio for
472 gismondine and phillipsite zeolites (1 for gismondine, 3 for phillipsite and ~1.7 for garronite).
473 Therefore, even if the garronite zeolite is not thermodynamically documented, the choice of
474 simulating its formation with gismondine and phillipsite is coherent.

475 The geochemical simulation results show that the same minerals formed during the
476 experiments were simulated during the geochemical exercise (Table 23). The characterization of
477 the carbonates formed is the same (e.g., calcite under 10% CO₂ / 90% N₂ and solid-solution of
478 Ca/Mg/Fe carbonate under 100% CO₂). Note that at the end of the experiment, the final pCO₂
479 ~~obtained by the geochemical simulation in the experiments with initial gas mixture of 100% CO₂~~
480 ~~and 10% CO₂ / 90% N₂ (calculated from the geochemical modeling results)~~ are equal to 0.79 and
481 0, ~~for initial gas mixture of 100% CO₂ and 10% CO₂ / 90% N₂~~ respectively. Zeolite is formed for
482 the 100% N₂ experiment in both the geochemical simulation and the experiments, ~~while for~~ the
483 10% CO₂ / 90% N₂ experiment, a minor amount is estimated during the geochemical simulation
484 ~~while, no zeolite is observed during the experiment~~ ~~this is not the case for the experimental part.~~
485 ~~Nevertheless, the amount estimated is low relative to the other minerals (1%). If zeolite was~~
486 ~~formed experimentally, it would be detected by XRD or NIR. The geochemical simulation results for the experiment~~
487 ~~time will have led to their formation.~~ Concerning geochemical simulation of the clay minerals, ~~as for the experimental~~
488 ~~results~~ mainly trioctahedral clay minerals are predicted (as for the experimental results) for the 100% N₂ experiment while mainly
489 dioctahedral phyllosilicates are predicted and observed ~~in the experiments during the experiments~~ involving CO₂. More
490 generally, the same overall trends are obtained between the experiments and the geochemical
491 simulation. Indeed, with the CO₂ % increase, the amount of trioctahedral phyllosilicates
492 decreases and the inverse trend is observed for the dioctahedral minerals. In the same manner, the

493 CO₂ % increase leads to a decrease in zeolite content and an increase in carbonate~~s~~ formation. The
494 pH values at the end of the experiments obtained by geochemical simulation are 6.3, 7.8 and 10.1
495 for the 100% CO₂, 10%CO₂ / 90% N₂ and 100% N₂ experiments, respectively. The final pH
496 values decrease with the increase of initial CO₂ %. To conclude, while there are noticeable
497 differences between the geochemical simulation and the experimental results, the same general
498 trends are observed with CO₂ % increase, which confirms the constraints, used and validates the
499 geochemical simulation.

500 5. Discussion

501 5.1 pH, a key to understanding mineral formation competition

502 The hydrothermal alteration of the tholeiitic volcanic glass, performed in this work,
503 produced ~~phyllosilicates clay minerals (di- and/or tri- octahedral, depending on the experimental~~
504 ~~conditions)~~, carbonates (with CO₂) and zeolites (initially CO₂-free). The minerals formed are in
505 line with previous experiments performed on tholeiitic basalt. Reaction products obtained from
506 experiments with various pCO₂ (from 1 to 35 bars) at various temperatures (from ambient to
507 250°C) on volcanic glass, contain trioctahedral smectites, chlorites, talc, carbonates and zeolites
508 [Declercq *et al.*, 2009; Gysi and Stefánsson, 2011; 2012a; b; c; Hellevang *et al.*, 2013; Stefánsson
509 and Gíslason, 2001]. The experimental conditions have been chosen to better understand the key
510 parameters driving zeolite and/or carbonate formation with trioctahedral minerals as observed on
511 Mars (Viviano-Beck *et al.* [2017]; Wray *et al.* [2016] and section 2 of this study). The initial
512 experimental conditions have a strong influence on whether such minerals form and the relative
513 amounts produced (Table 23). In order to grasp the factors involved in these mechanisms of
514 formation, geochemical modeling has been applied in this work.

515 Figure 3 presents the results of the geochemical modeling. ~~The~~ predicted mineral formed
516 ~~(in mol)~~ by the simulation (mineral in equilibrium with the aqueous solution during the
517 dissolution of the basaltic glass) and ~~the~~ percentage of dissolution (mol of basaltic glass dissolved
518 divided by the initial mol of basaltic glass) are plotted as a function of pH. We consider As, pH
519 ~~which is a~~ key parameter to understand the formation of these minerals from the weathering of
520 tholeiitic volcanic rock [Gysi and Stefánsson, 2012a; Stefánsson and Gíslason, 2001]. ~~Figure 3~~
521 ~~represents the evolution of the minerals formed (solid lines) as a function of pH for closed~~
522 ~~systems (atmosphere and aqueous solution are not renewed during the simulation). The mineral~~
523 ~~predicted and dissolution~~ evolutions vary between the experiments. This is driven by ~~and the~~
524 ~~% of dissolution (dashed grey lines) due to~~ the decrease of ~~the~~ CO₂ content in the available head-
525 space gases- (carbonation) and ~~due to~~ the release of the chemical elements from the dissolution of
526 the basaltic glass. The presence of CO₂ in the aqueous solution and in the head space controls the
527 pH of the aqueous solution, due to the dissociation of aqueous CO₂ into HCO₃⁻ + H⁺. Therefore,
528 the increase of the initial CO₂ % leads to a decrease of the initial pH (Figure 3). with pH ~~(6, 4.8,~~
529 ~~4.3 for the 100% N₂, 10% CO₂ / 90% N₂ and 100% CO₂ simulations, respectively).~~ During the
530 basaltic glass dissolution (represented by the % of dissolution, dotted grey lines, Figure 3), the
531 CO₂ present in the aqueous solution and in the head space are consumed by the carbonation as a
532 consequence the aqueous pH increase. The ~~(~~ final pCO₂ calculated from the geochemical
533 modelling results are equal at 0.32 and 0 for the 100% CO₂ and 10% CO₂ / 90% N₂, respectively;
534 ~~the pCO₂ were calculated from the geochemical modelling results).~~

535 During carbonation (Fig.3.I and II), di- and tri-octahedral phyllosilicates are formed with
536 a pH <~7.2, while when pH >~7.2 (after 12% of dissolution for 10% CO₂ / 90% N₂ and 100% N₂
537 simulation Figures 3.II and 3.III, respectively) the minerals formed are trioctahedral

538 phyllosilicates and zeolites. Therefore, the CO₂ % content has a strong influence on the
539 mechanism leading to the dioctahedral clay minerals, carbonate or zeolite formation. As seen by
540 the models dedicated to the 10% CO₂ / 90% N₂ experiments (Fig 3.II), the dioctahedral
541 phyllosilicates content increases until pH ~7.2 and then decreases in favor of zeolite content. The
542 increase of zeolite content is also accompanied by a decrease in the formation of carbonates.
543 These minerals are competing and the formation of one inhibits the formation of the other, such
544 as: dioctahedral clay minerals versus zeolites and carbonates versus zeolites (see figure 3.II).

545 ~~Indeed, t~~The increase in zeolite formation is due to both the availability of Ca²⁺ and due to
546 the decrease in formation of carbonates, which is accompanied by a pH increase (due to
547 carbonation) until pH ~7.2. That pH dependency has already been suggested as a key factor to
548 understand zeolite formation. In fact, *Burriesci et al.* [1984] argue that pH is a more important
549 factor than time and temperature. Moreover, as observed on soil on Earth, zeolite minerals are
550 generally described in neutral to basic soils [*Ming and Boettinger, 2001; Ming and Mumpton,*
551 *1989*]. Reciprocally, zeolites can be dissolved from soil samples by using acid treatments [*Ming*
552 *and Boettinger, 2001*]. Moreover, it is also described during the weathering process of basaltic
553 glass by geochemical modeling: a pH above 6.5 at 45°C leads to the formation of zeolite [*Gysi*
554 *and Stefánsson, 2012a*]. Indeed, the pH increase leads to the deprotonation of H₄SiO_{4(aq)} into
555 H₄SiO₃⁻ and H₄SiO₂²⁻ and to high cation/H₄⁺ ratios that are needed for the formation of zeolite
556 minerals [*Chipera and Apps, 2001; Ming and Boettinger, 2001; Mora-Fonz et al., 2007*].
557 Conversely, dioctahedral phyllosilicates are formed with pH <~7.2 in disfavor of zeolites (Figure
558 3, Table 23). This pH dependency could be a consequence of the incorporation of aluminum and
559 silica to build the framework of dioctahedral phyllosilicates and zeolites. The similarity between
560 zeolites and dioctahedral minerals are their structural formulae, notably regarding the

Formatted: Superscript

561 predominance of Si and Al. Even if no further explanation can be drawn from our study, it seems
562 that the silica and aluminum in solution plays a key role in mineral formation: pH <~7.2 lead to
563 dioctahedral phyllosilicates, while pH >~7.2 conditions lead to zeolites.

564 ~~Moreover, the~~ formation of trioctahedral ~~smeectite-clay~~ minerals ~~dedicated to Martian~~
565 ~~environments~~ does not appear to have strong pH dependency. ~~They can be formed~~ it is possible
566 ~~to form these~~ from both acidic ~~and basic conditions~~ (pH 4 ~~in~~; *Peretyazhko et al. [2016]*, ~~basic~~)
567 ~~and basic conditions~~ [*Tosca et al., [2008]*, ~~both~~ *Gysi and Stefánsson [2012a]*]. Nevertheless, for
568 the same temperature and alteration time, the content of Fe-rich trioctahedral chlorite increases
569 relative to the content of trioctahedral smectite with the increase of CO₂ % and ~~for acidity~~ (~~source~~
570 ~~of acidity could come from other aqueous species in the solution~~). ~~The source of acidity could~~
571 ~~either come from atmospheric gases or aqueous solution~~. Finally, the ratio between di- to tri-
572 octahedral minerals decreases with the pH increase and is therefore a good indicator of alteration
573 conditions.

574 The intrinsic parameter, which seems to govern the competition of formation between
575 dioctahedral phyllosilicates/ ~~versus~~ zeolites and carbonates/ ~~versus~~ zeolites, is pH. When the pH
576 is <~7.2, dioctahedral clay minerals are favored; while, when the pH is above 7.2, zeolites are
577 formed in disfavor of dioctahedral clay minerals. The competition between di- and tri-octahedral
578 phyllosilicates/carbonates/zeolites ~~competition~~ formation is a probe of the pH evolution of the
579 weathered solution. The association of dioctahedral phyllosilicates with carbonates will be an
580 indicator of acidic conditions, while the association of trioctahedral phyllosilicates with
581 carbonates will be an indicator of a fluid that could be acidic to < ~7.2. The indicator of basic
582 conditions is the association between trioctahedral phyllosilicates and zeolites. As consequence,

Formatted: Font: Italic

583 the association with trioctahedral phyllosilicates, carbonates and zeolites will indicate that the
584 weathering fluid has passed through pH \approx 7.2.

585 5.2 Martian implications

586 The results of this study are likely more relevant to understanding alteration by
587 hydrothermal fluids with different CO₂ % content rather than the impact of total atmospheric CO₂
588 levels. In closed system experiments, the CO₂ in the gas-head space is consumed during the
589 experiment, ~~and hence, the CO₂ levels herefore do es~~ not necessarily represent a CO₂ partial
590 pressure change, as suggested for the early Mars atmosphere evolution, because the real
591 atmosphere would buffer this level. ~~Nevertheless, c~~o-occurrence of carbonates and/or zeolites
592 with trioctahedral phyllosilicates has been observed on Martian Noachian crust (*Viviano-Beck et*
593 *al.* [2017]; *J. J. Wray et al.* [2016] and section 2). The geological formation process for such
594 mineral assemblages has putatively been assigned to hydrothermalism [*Brown et al.*, 2010;
595 *Ehlmann et al.*, 2011; *Niles et al.*, 2013; *Viviano et al.*, 2013]. The hydrothermal experimental
596 results obtained during this study are in line with previously discussed Martian observations
597 (Figure 1 and 2 and Table 23). Indeed, these two mineralogical assemblages have been formed
598 during the experiments under 100% N₂ and 10% CO₂ / 90% N₂.

599 The source of CO₂ levels in the hydrothermal fluids cannot be determined from this study,
600 but it could come from either the Martian atmosphere or magma [*Brown et al.*, 2010; *Bultel et al.*,
601 2015]. The hydrothermal experiments and their geochemical modeling show the strong link
602 between the formation of carbonates and zeolites during hydrothermal alteration in the presence
603 of CO₂. Due to the occurrence of trioctahedral phyllosilicates/carbonates and trioctahedral
604 phyllosilicates/zeolites at different conditions, a counter relationship between these two
605 assemblages (Al-phyllosilicates/zeolites and carbonates/zeolites) could certainly have existed

606 during early Mars. Thus, these reaction products can be used as an indicator for environmental
607 conditions due to the constraint given by their formation limits. Therefore, the observation of
608 trioctahedral phyllosilicates and zeolites on the Martian crust [Ehlmann *et al.*, 2009; Viviano-
609 Beck *et al.*, 2017] is an indicator of an alteration with an aqueous solution from a pH >
610 ~7.2, while the occurrence of trioctahedral clay minerals and carbonates is an indicator of slightly
611 acidic to ~7.2. Trioctahedral phyllosilicates associated with carbonates and zeolites were
612 observed in Valles Marineris [Viviano-Beck *et al.*, 2017] and impact craters [i.e.: Sun and
613 Milliken, 2015]. This mineralogical association is an indicator that the aqueous solution has
614 passed through a pH value of ~7.2 during the alteration process and perhaps in a closed
615 hydrothermal system.

616 The formation of trioctahedral phyllosilicates characterizes the major part of the Martian
617 weathered surface/outcrops formed in the Noachian ~~by~~ [Bibring *et al.* 2006]. However, here we
618 demonstrated that, with the wide [range of](#) aqueous CO₂ levels present during the experiments and
619 used in the geochemical simulations, trioctahedral phyllosilicates have never been formed alone.
620 Different studies without CO₂ involved have been able to produce trioctahedral minerals ~~by~~
621 ~~the~~ hydrothermal ~~alterationism~~ [alteration](#) of a volcanic glass and have pointed out that [specific](#) acidic
622 conditions (experiments using rock of basaltic composition, constant pH equal to ~4, Peretyazhko
623 *et al.* [2016]) are needed to form only trioctahedral minerals. Therefore, the widespread presence
624 of trioctahedral phyllosilicates (mainly smectitic) on Martian crust could imply acidic conditions
625 instead of a circum-neutral pH [Bibring *et al.*, 2006; Peretyazhko *et al.*, 2016]. Nevertheless, the
626 identification of zeolite when mixed with trioctahedral phyllosilicates (see section 2 of this
627 study), is difficult by NIR analysis. Therefore, the confirmation of the presence/absence of
628 zeolites (notably by lander/rover equipped with XRD, such as that on board the MSL mission)

629 with the widespread presence of trioctahedral phyllosilicates [Bibring *et al.*, 2006] is of prime
630 interest. It could imply drastically different environmental conditions during early Mars: acidic
631 and/or basic conditions. In addition, pH appears to be one of the most important parameters as a
632 driver of mineralogical competitions (in addition to silica activity for the formation of zeolites).
633 More experimental and geochemical modeling studies are required to investigate the clay
634 minerals/carbonates/zeolites competition. Indeed, other gases such as SO₂, which is considered
635 one of the important gases released during Martian volcanism [Cradock and Greeley, 2009], will
636 significantly modify the competitive behavior.

637 Interestingly, when the percentage of aqueous CO₂ increases and consequently the pH
638 decreases, the content of trioctahedral chlorite increases in disfavor of the trioctahedral smectite
639 content (Figure 1 and 2). The observation on the relative content of chlorite compared to smectite
640 as a function of depth (Bultel *et al.* [2015]; Carter *et al.* [2013]; Loizeau *et al.* [2012]; Sun and
641 Milliken [2015]) could not only be related to burial diagenesis on Mars [Sun and Milliken, 2015],
642 but also to fluid composition during hydrothermal alteration. Further experiments dedicated to
643 this transformation using infrared and XRD characterization of the smectite/chlorite relative
644 amounts in MLM will bring more constraints to the processes which led to this specific
645 observation.

646 **Conclusion and remarks**

647 ~~In the present study, we have investigated the di/tri octahedral clay~~
648 ~~minerals/carbonates/zeolites relationship to better understand the early aqueous alteration in~~
649 ~~Martian history. Indeed~~ On Mars, widespread occurrence of Fe,Mg-phyllosilicates have been
650 observed by remote sensing instruments on Noachian terrains. Experimental investigations had
651 shown that their conditions formations could be widespread in terms of pH range, oxic/anoxic

652 conditions, etc... Thus, the present study is dedicated to better constraint the formation conditions
653 of clay minerals by using other minerals found in association with them on the Martian surface.
654 While Fe,Mg clay minerals are the main minerals observed, carbonates and zeolites were also
655 detected always associated with Fe/Mg phyllosilicates. Here, we report on the dioctahedral
656 versus zeolites and carbonates versus zeolites formation to better define the early Mars alteration
657 history, always associated with Fe/Mg phyllosilicates or can occur with both zeolites and Fe/Mg
658 phyllosilicates. ~~Hydrothermal~~ Hydrothermal experiments on a tholeiitic volcanic glass were
659 performed, ~~in this study,~~ in a closed system with a water-rock ratio of 20 and a head space of 520
660 ml. Three different initial gas mixtures with various CO₂ contents were used in the experiments:
661 100% CO₂, 10% CO₂ / 90 % N₂ and 100 % N₂. The minerals formed during the experiments were
662 characterized by XRD and NIR analyses. Complementary geochemical modeling was done to
663 reproduce the different experiments to establish the parameter driving the mineralogical
664 formation. The experimental results show that ~~W~~with the decrease of CO₂ percentage, the content
665 of dioctahedral clay minerals decreases in favor of trioctahedral minerals and zeolites. Carbonates
666 are formed during the experiments containing CO₂ while zeolite is formed with a CO₂-free fluid.
667 The geochemical simulation provides insight into the aqueous alteration environment as a
668 function of the mineral association. Three mineralogical associations could be used to follow the
669 pH conditions during the alteration. Indeed, ~~d~~dioctahedral clay minerals and carbonate minerals
670 are formed under pH <~7.2 (at 120°C)acidic conditions, and trioctahedral-Trioctahedral minerals
671 are formed with carbonates from pH >6 (at 120°C)neutral pH aqueous solutions.
672 Moreover,Finally, trioctahedral clay minerals and zeolites are formed with a pH >~7.2.

673 Moreover,In addition, ~~the~~ the results obtained here show that the relative content of
674 trioctahedral chlorite compares to trioctahedral /smectite increase with ~~de~~ decrease of acidity.

Formatted: Indent: First line: 1.27 cm

675 Hence, the relative content of chlorite and smectite could not only have been related to burial
676 diagenesis, but may also be a result of differing acidic fluids. More experiments and geochemical
677 modeling using different fluids or /atmosphere compositions (rich in SO₂, for example) will help
678 to better define the mineral competition behavior and, therefore, to grasp the aqueous and
679 alteration processes of early Mars.

680 **Acknowledgements**

681 This work was partly supported by the Research Council of Norway through its Centre of
682 Excellence funding scheme, project number 223272. This project has received funding from the
683 European Union's Horizon 2020 (H2020-COMPET-2015) research and innovation programme
684 under grant agreement No 687302 (PTAL). This study is supported by the Research Council of
685 Norway (235058/F20 CRATER CLOCK). L. Riu acknowledges the IDEX Université Paris-
686 Saclay for her PhD grant. The authors would like to thank Thanusha Naidoo for correcting the
687 English, Christian Sætre, Mufak Said Naoroz, Rune Bjørnestøl Per-Olav Korsmo for laboratory
688 help and Helge Hellevang, Henning Dypvik for providing the sample. Finally, the authors wish to
689 acknowledge the editor Dr. D. Baratoux, as well as Dr. H. Newsom and two anonymous
690 reviewers, for their constructive comments that greatly improved the quality of this work. All
691 data used to characterize our initial and altered samples are included in the figures, tables, and
692 supporting information of this manuscript.

693 **Figure caption**

694 **Figure 1:** Bulk XRD patterns between 2-55 °2θ and NIR spectra of the unreacted basalt
695 (I.a and II.a, respectively), ~~bulk XRD patterns and NIR spectra and~~ of the weathered basalt under
696 100% CO₂ (I.b and II.b, respectively), under 10% CO₂ / 90% N₂ (I.c and II.c, respectively) and
697 under 100% N₂ (I.d and II.d, respectively). ~~The triangles, the diamonds and the~~ stars represent the
698 XRD peaks of forsterite, pyroxene and quartz respectively. From low to high angles, the peak
699 position corresponding to: the triangles are at 5.12, 3.89, 3.50, 2.78, 2.52, 2.47, 2.36, 2.27, 2.56,
700 2.17 and 1.75 Å; to the stars are at 4.26 and 3.33 Å; and to the diamonds are at 3.20 and 2.99 Å

701 **Figure 2:** Comparison of the XRD patterns recorded on oriented preparation obtained in
702 Ca-AD (black line) and Ca-EG (grey line) states for the weathered basalt under 100% N₂ (I.c),
703 under 10% CO₂/90% N₂ (I.b) and under 100% CO₂ (I.a). Comparison of the XRD patterns
704 recorded on oriented preparations obtained in Ca-AD (black line), K-110 (grey line), K-330 (blue
705 line) and K-550 (red line) states for the weathered basalt under 100% N₂ (II.c), under
706 10% CO₂/90% N₂ (II.b) and under 100% CO₂ (II.a). Comparison of the NIR spectra continuum
707 removed for the weathered basalt under 100% N₂ (III.c), under 10% CO₂/90% N₂ (III.b) and
708 under 100% CO₂ (III.a).

709 **Figure 3:** Geochemical results obtained from the dissolution of the basaltic glass for the
710 100% N₂ (I), 10% CO₂ / 90% N₂ (II) and 100% CO₂ (III) simulation as a function of pH.

711

Formatted: Subscript

Formatted: Subscript

Formatted: Subscript

712 **Tables**

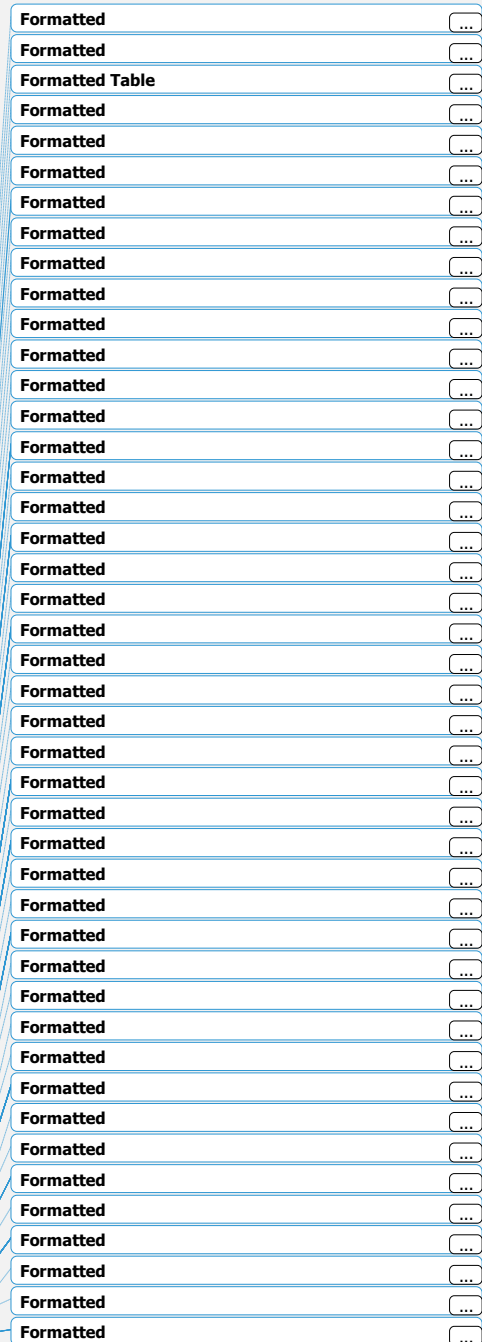
713 **Table 1:** Total chemistry in oxides, the related calculated structural formulae and the
 714 Log(K) values of the original basalt used in the present study.

Oxides	SiO ₂	Al ₂ O ₃	Fe ₂ O ₃ (T)	MgO	NaO	K ₂ O	CaO	
%	48.2	14.2	12.0	9.4	1.9	0.3	11.7	
Elements	Si	Al	Fe	Mg	Na	K	Ca	O
mol	1	0.35	0.23	0.29	0.01	0.07	0.26	3.345
Temperature (°C)	0	25	60	100	150	200	250	300
Log(K)	18.10	16.30	13.86	11.59	9.28	7.37	5.71	4.21

715

716 ~~Table 2: List of minerals and solid solution added during the geochemical simulation to~~
 717 ~~account of the lack of the original at the data0.cmp data base (from EQ3/6 software).~~ **Table 2:**
 718 List of minerals, and solid-solution added and suppressed during the geochemical simulation to
 719 account of the lack of the original at the data0.cmp data base (from EQ3/6 software).

Minerals / Solid-solutions	Structural formulae
<u>Trioctahedral clay minerals:</u>	
<u>Saponite</u>	$(Ca,Mg,Na_2,K_2)_{0.17}(Mg_3)(Al_{0.34}Si_{3.66})O_{10}(OH)_2$
<u>Fe-rich saponite</u>	$(Ca,Mg,Na_2,K_2)_{0.17}(Fe,Mg_2)(Al_{0.34}Si_{3.66})O_{10}(OH)_2$
<u>Tri-chlorite</u>	$(Fe,Mg)_5Al_2Si_3O_{10}(OH)_8$
<u>Talcs</u>	$(Mg,Fe)_3Si_4O_{10}(OH)_2$
<u>Diocahedral clay minerals:</u>	
<u>Montmorillonite</u> Montmorillonites	$(Mg,Ca,Na_2,K_2)_{0.165}(Mg_{0.33}Al_{1.67})Si_4O_{10}(OH)_2$
<u>Nontronites</u>	$(Mg,Ca,Na_2,K_2)_{0.165}(Fe_2)(Al_{0.33}Si_{3.67})O_{10}(OH)_2$
<u>Beidellites</u>	$(Mg,Ca,Na_2,K_2)_{0.17}Al_{2.34}Si_{3.66}O_{10}(OH)_2$
<u>Kaolinite</u>	$Al_2Si_2O_5(OH)_4$
<u>Di-chlorites</u> Fe-sudoite	$(Fe,Mg)_2Al_4Si_3O_{10}(OH)_8$
<u>Vermiculite</u> Vermiculites	$(Ca,Mg,Na_2,K_2)_{0.43}(Mg_3)(Al_{0.43}Si_{3.14})O_{10}OH_2$
<u>Illite</u> Illites	$K_{0.85}(Mg,Fe)_{0.25}Al_{2.35}Si_{3.4}O_{10}(OH)_2$
<u>Zeolites</u> Phillipsite	
<u>Phillipsites</u>	$(Ca,N_2,K_2)_{0.5}AlSi_3O_8 \cdot 3H_2O$
<u>Gismondine</u>	$Ca_2Al_4Si_4O_{16} \cdot 9H_2O$
<u>Clinoptilolites</u>	$(Ca,Na_2,K_2)_{0.55}(Si_{4.9}Al_{1.1})O_{12} \cdot 3.9H_2O$
<u>Heulandites</u>	$(Ca,Na_2)_{11}Al_2Si_7O_{18} \cdot 5H_2O$
<u>Mordenite</u>	$Ca_{0.2895}Na_{0.361}Al_{0.94}Si_{5.06}O_{12} \cdot 3.468H_2O$
<u>Stellerite</u>	$Ca_2Al_4Si_{14}O_{36} \cdot 14H_2O$



<u>Natrolites</u>	<u>$(Ca,Na_2)Al_2Si_3O_{10} \cdot 3H_2O$</u>
Carbonates	<u>$(Ca,Mg,Fe)CO_3$</u>
Suppressed minerals	Reason why
<u>prehnite, olivine, magnetite, biotite, graphite,</u> <u>wollastonite, amphibole and epidote</u>	<u>Formed in higher/pressure ranges</u>
<u>akermanite, monticellite and merwinite</u>	<u>Formed in metamorphosed sediments</u>
<u>Serpentines</u>	<u>Formed from olivine dissolution</u>

720

721

722

723

724

725

Table 23: Summary of the experimental results and mol of minerals predicted by the geochemical modeling at the same rate of dissolution as a function of the gas composition.

726

^a The percentage of dissolution of the basaltic glass has been estimated by XRD with an uncertainty of ± 2 % (for more details see section 4.1)

728

^b The trioctahedral minerals correspond to the sum of trioctahedral smectite, trioctahedral chlorite and talc.

730

^c The dioctahedral minerals correspond to the sum of dioctahedral smectite, kaolinite and illite.

732

^d The carbonates are expressed as a solid solution between the proportion of calcite (Ca), magnesite (Mg) and siderite (Fe).

734

^e The zeolites correspond to garronite for the experiments and to the sum of gismondine and phillipsite for the geochemical modeling (for more details see section 4.1 and 4.2).

735

Formatted: Norwegian (Bokmål)

Formatted: Norwegian (Bokmål)

Formatted: Norwegian (Bokmål), Subscript

Formatted: Norwegian (Bokmål)

Formatted: Line spacing: single

Formatted: Norwegian (Bokmål), Subscript

Formatted: Norwegian (Bokmål)

Formatted: Line spacing: single

Formatted: Subscript

Formatted: Line spacing: single

Formatted: Line spacing: single

Formatted: Line spacing: single

Formatted: Line spacing: single

736 -, +, ++, +++ represent the relative abundance of the minerals (based on peak intensities)

737 between the different atmospheres from non-present to the highest relative proportion.

Experiments / Simulation names	Dissolution % ^a (±2 %)	Minerals						Zeolites ^e (simulated)	pH
		Experiments / Geochemical modeling (.10 ⁻⁴ mol)			Carbonates (Ca/Mg/Fe) % ^d				
		Trioctahedral ^b	Diocahedral ^c						
100% N ₂	19	+++	9.9	-	0.2	-	-	+ 4.5	<u>10.1</u>
10% CO ₂ / 90% N ₂	23	++	6.6	+	9.4	+	16.6 (97/2/1)	- 2.8	<u>7.8</u>
100% CO ₂	25	+	5.6	++	20.1	+	35.9 (68/20/12)	- -	<u>6.3</u>

Formatted Table

738

739 **Bibliography**

- 740 Agee, C. B., et al. (2013), Unique Meteorite from Early Amazonian Mars: Water-Rich
741 Basaltic Breccia Northwest Africa 7034, *Science (New York, N.Y.)*, doi:10.1126/science.1228858.
- 742 Ansan, V., D. Loizeau, N. Mangold, S. Le Mouélic, J. Carter, F. Poulet, G. Dromart, A.
743 Lucas, J.-P. Bibring, and A. Gendrin (2011), Stratigraphy, mineralogy, and origin of layered
744 deposits inside Terby crater, Mars, *Icarus*, 211(1), 273-304.
- 745 Aradóttir, E. S. P., E. L. Sonnenthal, and H. Jónsson (2012), Development and evaluation
746 of a thermodynamic dataset for phases of interest in CO₂ mineral sequestration in basaltic rocks,
747 *Chemical Geology*, 304–305, 26-38, doi:http://dx.doi.org/10.1016/j.chemgeo.2012.01.031.
- 748 Bandfield, J. L., T. D. Glotch, and P. R. Christensen (2003), Spectroscopic identification
749 of carbonate minerals in the Martian dust, *Science (New York, N.Y.)*, 301(5636), 1084-1087.
- 750 Barnishel R. I. and P. M. Bertsch (1989) Chlorites and hydroxy-interlayered vermiculite
751 and smectite. In *Minerals in Soil Environments Soil Science Society of America, Madison*. pp.
752 729–788.
- 753 Baron F., S. Petit, E. Tertre and A. Decarreau (2017) Influence of aqueous Si and Fe
754 speciation on tetrahedral Fe(III) substitutions on nontronites: a clay synthesis approach, *Clays
755 and Clay Minerals, Vol. 64, No. 3*, 230–244.
- 756 Bibring, J. P., et al. (2006), Global mineralogical and aqueous mars history derived from
757 OMEGA/Mars Express data, *Science (New York, N.Y.)*, 312(5772), 400-404,
758 doi:10.1126/science.1122659.
- 759 Bishop, J. L., C. M. Pieters, and J. O. Edwards (1994), Infrared spectroscopic analyses on
760 the nature of water in montmorillonite, *Clays and Clay Minerals*, 42(6), 702-716.
- 761 Bishop, J. L., M. D. Lane, M. D. Dyar and A. J. Brown (2008), Reflectance and emission
762 spectroscopy study of four groups of phyllosilicates: smectites, kaolinite-serpentines, chlorites
763 and micas, *Clay minerals*, 43(1), 35-54.
- 764 Blanc, P. (2009), Thermochimie – Sélection de constantes thermodynamiques pour
765 les zéolites : version 2. Rapport final. *Rep.*, 55 pp, BRGM.
- 766 Boynton, W. V., et al. (2007), Concentration of H, Si, Cl, K, Fe, and Th in the low- and
767 mid-latitude regions of Mars, *Journal of Geophysical Research: Planets*, 112(E12-S99),
768 doi:10.1029/2007JE002887.
- 769 Brasier, M. D., R. Matthewman, S. McMahon, and D. Wacey (2011), Pumice as a
770 remarkable substrate for the origin of life, *Astrobiology*, 11(7), 725-735.
- 771 Brown, A. J., S. J. Hook, A. M. Baldridge, J. K. Crowley, N. T. Bridges, B. J. Thomson,
772 G. M. Marion, C. R. de Souza Filho, and J. L. Bishop (2010), Hydrothermal formation of Clay-
773 Carbonate alteration assemblages in the Nili Fossae region of Mars, *Earth and Planetary Science
774 Letters*, 297(1–2), 174-182, doi:http://dx.doi.org/10.1016/j.epsl.2010.06.018.

775 Bultel, B., C. Quantin-Nataf, M. Andréani, H. Clénet, and L. Lozac'h (2015), Deep
776 alteration between Hellas and Isidis Basins, *Icarus*, 260, 141-160,
777 doi:<http://dx.doi.org/10.1016/j.icarus.2015.06.037>.

778 Burriesci, N., M. L. Crisafulli, N. Giordano, and J. C. J. Bart (1984), Factors affecting
779 formation of zeolite a from aluminosilicate gels, *Materials Letters*, 2(5), 401-406,
780 doi:[http://dx.doi.org/10.1016/0167-577X\(84\)90120-4](http://dx.doi.org/10.1016/0167-577X(84)90120-4).

781 Carter, J., F. Poulet, J. Bibring, S. Murchie, V. Ansan, and N. Mangold (2010),
782 Mineralogy of Layered Deposits in Terby Crater, N. Hellas Planitia, paper presented at Lunar and
783 Planetary Institute Science Conference Abstracts.

784 Carter, J., F. Poulet, J. P. Bibring, N. Mangold, and S. Murchie (2013), Hydrous minerals
785 on Mars as seen by the CRISM and OMEGA imaging spectrometers: Updated global view,
786 *Journal of Geophysical Research: Planets*, 118(4), 831-858.

787 Carter, J., D. Loizeau, N. Mangold, F. Poulet, and J.-P. Bibring (2015), Widespread
788 surface weathering on early Mars: A case for a warmer and wetter climate, *Icarus*, 248, 373-382,
789 doi:<http://dx.doi.org/10.1016/j.icarus.2014.11.011>.

790 Catalano, J. G. (2013), Thermodynamic and mass balance constraints on iron-bearing
791 phyllosilicate formation and alteration pathways on early Mars, *J. Geophys. Res. E Planets*,
792 118(10), 2124-2136, doi:10.1002/jgre.20161

793 Chevrier, V., F. Poulet, and J.-P. Bibring (2007), Early geochemical environment of Mars
794 as determined from thermodynamics of phyllosilicates, *Nature*, 448(7149), 60-63,
795 doi:http://www.nature.com/nature/journal/v448/n7149/supinfo/nature05961_S1.html.

796 Chipera S. and J. A. Apps (2001) Geochemical Stability of Natural Zeolites, *Reviews in*
797 *mineralogy and geochemistry*, 45(1), 117-157.

798 Chipera, S., and D. Bish (2013), Fitting Full X-Ray Diffraction Patterns for Quantitative
799 Analysis: A Method for Readily Quantifying Crystalline and Disordered Phases, *Advances in*
800 *Materials Physics and Chemistry*, 3(1A), 47-53.

801 Clark, R. N., A. J. Gallagher, and G. A. Swayze (1990), Material Absorption Band Depth
802 Mapping of Imaging Spectrometer Data Using a Complete Band Shape Least-Squares Fit with
803 Library Reference Spectra, Proceedings of the Second Airborne Visible/Infrared Imaging
804 Spectrometer (AVIRIS)

805 Cloutis, E. A., P. M. Asher and S. A. Mertzman (2002), Spectral reflectance properties of
806 zeolites and remote sensing implications. *Journal of Geophysical Research: Planets*, 107(E9).

807 Craddock R.A. and R. Greeley (2009), Minimum estimates of the amount and timing of
808 gases released into the martian atmosphere from volcanic eruptions, *Icarus*, 204(2), 512-526.

809 Declercq, J., H. Dypvik, P. Aagaard, J. Jahren, R. E. Ferrell, and J. W. Horton (2009),
810 Experimental alteration of artificial and natural impact melt rock from the Chesapeake Bay
811 impact structure, *Geological Society of America Special Papers*, 458, 559-569.

812 Dehouck, E., A. Gaudin, N. Mangold, L. Lajaunie, A. Dauzères, O. Grauby, and E. Le
813 Menn (2014), Weathering of olivine under CO₂ atmosphere: A martian perspective, *Geochim.*
814 *Cosmochim. Acta*, 135, 170-189, doi:10.1016/j.gca.2014.03.032.

815 Dehouck, E., A. Gaudin, V. Chevrier, and N. Mangold (2016), Mineralogical record of
816 the redox conditions on early Mars, *Icarus*, 271, 67-75, doi:10.1016/j.icarus.2016.01.030.

817 Dlugogorski B. Z. and R. D. Balucan (2014), Dehydroxylation of serpentine minerals:
818 Implications for mineral carbonation, *Renewable and Sustainable Energy Reviews*, 31, 353-367.

819 Dyer, A. (2002), Natural Zeolites: Occurrences, Properties, Applications., *Clay Minerals*,
820 37(4), 733.

821 Ehlmann, B. L., J. F. Mustard, S. L. Murchie, F. Poulet, J. L. Bishop, A. J. Brown, W. M.
822 Calvin, R. N. Clark, D. J. Des Marais, and R. E. Milliken (2008), Orbital identification of
823 carbonate-bearing rocks on Mars, *Science (New York, N.Y.)*, 322(5909), 1828-1832.

824 Ehlmann, B. L., J. F. Mustard, G. A. Swayze, R. N. Clark, J. L. Bishop, F. Poulet, D. J.
825 Des Marais, L. H. Roach, R. E. Milliken, and J. J. Wray (2009), Identification of hydrated silicate
826 minerals on Mars using MRO-CRISM: Geologic context near Nili Fossae and implications for
827 aqueous alteration, *Journal of Geophysical Research: Planets*, 114(E2).

828 Ehlmann, B. L., J. F. Mustard, S. L. Murchie, J.-P. Bibring, A. Meunier, A. A. Fraeman,
829 and Y. Langevin (2011), Subsurface water and clay mineral formation during the early history of
830 Mars, *Nature*, 479(7371), 53-60.

831 Fernández-Remolar, D. C., M. Sánchez-Román, A. C. Hill, D. Gómez-Ortíz, O. P.
832 Ballesteros, C. S. Romanek, and R. Amils (2011), The environment of early Mars and the
833 missing carbonates, *Meteoritics & Planetary Science*, 46(10), 1447-1469, doi:10.1111/j.1945-
834 5100.2011.01238.x.

835 Gaffey, S. J. (1985), Reflectance spectroscopy in the visible and near-infrared (0.35–2.55
836 μm): Applications in carbonate petrology, *Geology*, 13(4), 270-273.

837 Gellert, R., et al. (2006), Alpha Particle X-Ray Spectrometer (APXS): Results from
838 Gusev crater and calibration report, *Journal of Geophysical Research: Planets (1991–2012)*,
839 111(E2), doi:10.1029/2005JE002555.

840 Gooding, J. L. (1992), Soil mineralogy and chemistry on Mars: Possible clues from salts
841 and clays in SNC meteorites, *Icarus*, 99(1), 28-41.

842 Griffith, L. L., and E. L. Shock (1995), A geochemical model for the formation of
843 hydrothermal carbonates on Mars, *Nature*, 377(6548), 406-408.

844 Gysi, A. P., and A. Stefánsson (2011), CO₂–water–basalt interaction. Numerical
845 simulation of low temperature CO₂ sequestration into basalts, *Geochim. Cosmochim. Acta*,
846 75(17), 4728-4751, doi:http://dx.doi.org/10.1016/j.gca.2011.05.037.

847 Gysi, A. P., and A. Stefánsson (2012a), CO₂-water–basalt interaction. Low temperature
848 experiments and implications for CO₂ sequestration into basalts, *Geochim. Cosmochim. Acta*, 81,
849 129-152, doi:http://dx.doi.org/10.1016/j.gca.2011.12.012.

850 Gysi, A. P., and A. Stefánsson (2012b), Experiments and geochemical modeling of CO₂
851 sequestration during hydrothermal basalt alteration, *Chemical Geology*, 306–307, 10-28,
852 doi:http://dx.doi.org/10.1016/j.chemgeo.2012.02.016.

853 Gysi, A. P., and A. Stefánsson (2012c), Mineralogical aspects of CO₂ sequestration
854 during hydrothermal basalt alteration — An experimental study at 75 to 250 °C and elevated
855 pCO₂, *Chemical Geology*, 306–307, 146-159,
856 doi:http://dx.doi.org/10.1016/j.chemgeo.2012.03.006.

857 Hay, R. L., and R. A. Sheppard (2001), Occurrence of zeolites in sedimentary rocks: An
858 overview, *Reviews in mineralogy and geochemistry*, 45(1), 217-234.

859 Hellevang, H., H. Dypvik, E. Kalleson, L. Pittarello, and C. Koeberl (2013), Can
860 alteration experiments on impact melts from El'gygytgyn and volcanic glasses shed new light on
861 the formation of the Martian surface?, *Meteoritics & Planetary Science*, 48(7), 1287-1295,
862 doi:10.1111/maps.12046.

863 Hunt, G. R., and J. W. Salisbury (1970), Visible and near-infrared spectra of minerals and
864 rocks, I. Silicate minerals, *Modern geology*, 1, 283-300.

865 Hunt, G. R. (1977), Spectral signatures of particulate minerals in the visible and near
866 infrared, *Geophysics*, 42(3), 501-513.

867 Iriarte I., S. Petit, F. J. Huertas, S. Fiore, O. Grauby, A. Decarreau and J. Âlinares(2005)
868 Synthesis of Kaolinite with a High Level of Fe³⁺ for Al substitution, *Clays and Clay Minerals*,
869 Vol. 53, No. 1, 1-10, 2005.

870 King, T. V. and R. N. Clark, (1989) Spectral characteristics of chlorites and Mg-
871 serpentines using high-resolution reflectance spectroscopy. *Journal of Geophysical Research:*
872 *Solid Earth*, 94(B10), 13997-14008.

873 Kralj, P., S. Rychagov, and P. Kralj (2010), Zeolites in volcanic-igneous hydrothermal
874 systems: a case study of Pauzhetka geothermal field (Kamchatka) and Oligocene Smrekovec
875 volcanic complex (Slovenia), *Environmental Earth Sciences*, 59(5), 951-956,
876 doi:10.1007/s12665-009-0249-4.

877 Liu, Y., and J. G. Catalano (2016), Implications for the aqueous history of southwest
878 Melas Chasma, Mars as revealed by interbedded hydrated sulfate and Fe/Mg-smectite deposits,
879 *Icarus*, 271, 283-291, doi:http://dx.doi.org/10.1016/j.icarus.2016.02.015.

880 Lodders, K. (1998), A survey of shergottite, nakhlite and chassigny meteorites whole-rock
881 compositions, *Meteoritics & Planetary Science*, 33(S4), A183-A190, doi:10.1111/j.1945-
882 5100.1998.tb01331.x.

883 Loizeau, D., J. Carter, S. Bouley, N. Mangold, F. Poulet, J.-P. Bibring, F. Costard, Y.
884 Langevin, B. Gondet, and S. L. Murchie (2012), Characterization of hydrated silicate-bearing
885 outcrops in Tyrrenha Terra, Mars: Implications to the alteration history of Mars, *Icarus*, 219(1),
886 476-497.

887 Matter, J. M., et al. (2016), Rapid carbon mineralization for permanent disposal of
888 anthropogenic carbon dioxide emissions, *Science (New York, N.Y.)*, 352(6291), 1312-1314,
889 doi:10.1126/science.aad8132.

890 McSween, H. Y. (1994), What we have learned about Mars from SNC meteorites,
891 *Meteoritics*, 29(6), 757-779.

892 McSween, H. Y., M. B. Wyatt, R. Gellert, J. Bell, R. V. Morris, K. E. Herkenhoff, L. S.
893 Crumpler, K. A. Milam, K. R. Stockstill, and L. L. Tornabene (2006), Characterization and
894 petrologic interpretation of olivine-rich basalts at Gusev Crater, Mars, *Journal of Geophysical*
895 *Research: Planets*, 111(E2).

896 McSween, H. Y., G. J. Taylor, and M. B. Wyatt (2009), Elemental composition of the
897 Martian crust, *Science (New York, N.Y.)*, 324(5928), 736-739.

898 Meunier, A., S. Petit, C. S. Cockell, A. El Albani, and D. Beaufort (2010), The Fe-rich
899 clay microsystems in basalt-komatiite lavas: importance of Fe-smectites for pre-biotic molecule
900 catalysis during the Hadean Eon, *Origins of Life and Evolution of Biospheres*, 40(3), 253-272.

901 Ming, D. W. and J. L. Gooding (1988), Zeolites on Mars: Possible environmental
902 indicators in soils and sediments, *In Lunar and Planetary Inst., Workshop on Mars Sample*
903 *Return Science*, 124-125.

904 Ming, D. W., and F. A. Mumpton (1989), Zeolites in Soils, in *Minerals in Soil*
905 *Environments*, edited by J. B. Dixon and S. B. Weed, pp. 873-911, Soil Science Society of
906 America, Madison, WI, doi:10.2136/sssabookser1.2ed.c18.

907 Ming, D. W., and J. L. Boettlinger (2001), Zeolites in soil environments, *Reviews in*
908 *mineralogy and geochemistry*, 45(1), 323-345.

909 Ming, D. W., et al. (2008), Geochemical properties of rocks and soils in Gusev Crater,
910 Mars: Results of the Alpha Particle X-Ray Spectrometer from Cumberland Ridge to Home Plate,
911 *Journal of Geophysical Research: Planets (1991–2012)*, 113(E12), doi:10.1029/2008JE003195.

912 Morse, J. W. and Marion, G. M. (1999). The role of carbonates in the evolution of early
913 Martian oceans. *American Journal of Science*, 299(7-9), 738-761.

914 Mousis, O., J.-M. Simon, J.-P. Bellat, F. Schmidt, S. Bouley, E. Chassefière, V. Sautter,
915 Y. Quesnel, S. Picaud, and S. Lectez (2016), Martian zeolites as a source of atmospheric
916 methane, *Icarus*, 278, 1-6, doi:http://dx.doi.org/10.1016/j.icarus.2016.05.035.

917 Mora-Fonz M. J., C. Richard A. Catlow, and D. W. Lewis (2007), Modeling Aqueous
918 silica Chemistry in Alkali Media, *J. Phys. Chem. C*, *111* (49), 18155–18158, doi:
919 10.1021/jp077153u.

920 Mustard, J. F., (1992), Chemical composition of actinolite from reflectance
921 spectra, *American Mineralogist* *77*, 345-358

922 Niles, P. B., D. C. Catling, G. Berger, E. Chassefière, B. L. Ehlmann, J. R. Michalski, R.
923 Morris, S. W. Ruff, and B. Sutter (2013), Geochemistry of Carbonates on Mars: Implications for
924 Climate History and Nature of Aqueous Environments, *Space Science Reviews*, *174*(1), 301-328,
925 doi:10.1007/s11214-012-9940-y.

926 Pajola, M., S. Rossato, J. Carter, E. Baratti, R. Pozzobon, M. S. Erculiani, M. Coradini,
927 and K. McBride (2016), Eridania Basin: An ancient paleolake floor as the next landing site for
928 the Mars 2020 rover, *Icarus*, *275*, 163-182.

929 Paul, A. (1977), Chemical durability of glasses; a thermodynamic approach, *Journal of*
930 *Materials Science*, *12*(11), 2246-2268, doi:10.1007/bf00552247.

931 Peretyazhko, T. S., B. Sutter, R. V. Morris, D. G. Agresti, L. Le, and D. W. Ming (2016),
932 Fe/Mg smectite formation under acidic conditions on early Mars, *Geochim. Cosmochim. Acta*,
933 *173*, 37-49, doi:http://dx.doi.org/10.1016/j.gca.2015.10.012.

934 Petit S. and A. Decarreau (1990), Hydrothermal (200°C) synthesis and crystal chemistry
935 of iron-rich kaolinites, *Clay Minerals*, *Vol 25*, 181-196.

936 Petit S. and J. Madejova (2013), *Handbook of Clay Science Part B*, Chapter 2.7, Elsevier.

937 Petit S., A. Decarreau, W. Gates, P. Andrieux and O. Grauby (2015), Hydrothermal
938 synthesis of dioctahedral smectites: The Al–Fe³⁺ chemical series. Part II: Crystal-chemistry,
939 *Applied Clay Science*, *Vol 104*, 96–105.

940 Pollack, J. B., J. F. Kasting, S. M. Richardson, and K. Poliakov (1987), The case for a
941 wet, warm climate on early Mars, *Icarus*, *71*(2), 203-224.

942 Ruff, S. W. (2004), Spectral evidence for zeolite in the dust on Mars, *Icarus*, *168*(1), 131-
943 143.

944 Stefánsson, A., and S. R. Gíslason (2001), Chemical Weathering of Basalts, Southwest
945 Iceland: Effect of Rock Crystallinity and Secondary Minerals on Chemical Fluxes to the Ocean,
946 *American Journal of Science*, *301*(6), 513-556, doi:10.2475/ajs.301.6.513.

947 [Stockmann G., Wolff-Boehnisch D., Gíslason S.R. and E.H. Oelkers \(2008\) Dissolution of](#)
948 [diopside and basaltic glass: the effect of carbonate coating, *Mineralogical Magazine*, *72*\(1\), 135-](#)
949 [139.](#)

950 Sun, V. Z., and R. E. Milliken (2015), Ancient and recent clay formation on Mars as
951 revealed from a global survey of hydrous minerals in crater central peaks, *Journal of Geophysical*
952 *Research: Planets*, 120(12), 2293-2332, doi:10.1002/2015JE004918.

953 Tomita, K., H. Yamane, and M. Kawano (1993), Synthesis of smectite from volcanic
954 glass at low temperature, *Clays and Clay Minerals*, 41, 655-655.

955 Tomkinson, T., M. R. Lee, D. F. Mark, and C. L. Smith (2013), Sequestration of Martian
956 CO₂ by mineral carbonation, *Nature communications*, 4.

957 Tosca, N., R. Milliken, and F. Michel (2008), Smectite formation on early Mars:
958 Experimental constraints, *LPI Contributions*, 1441, 77-78.

959 Utada (1988), Hydrothermal alteration envelope relating to Kuroko-type mineralization: a
960 review., *Mining Geol.*, 12, 79-92.

961 van Bekkum, H., and H. W. Kouwenhoven (1989), The use of zeolites in organic
962 reactions, *Recueil des Travaux Chimiques des Pays-Bas*, 108(9), 283-294,
963 doi:10.1002/recl.19891080902.

964 Venuto, P. B. (1994), Organic catalysis over zeolites: A perspective on reaction paths
965 within micropores, *Microporous Materials*, 2(5), 297-411, doi:http://dx.doi.org/10.1016/0927-
966 6513(94)00002-6.

967 Viviano, C. E., J. E. Moersch, and H. Y. McSween (2013), Implications for early
968 hydrothermal environments on Mars through the spectral evidence for carbonation and
969 chloritization reactions in the Nili Fossae region, *Journal of Geophysical Research: Planets*,
970 118(9), 1858-1872, doi:10.1002/jgre.20141.

971 Viviano-Beck, C. E., S. L. Murchie, A. W. Beck, and J. M. Dohm (2017), Compositional
972 and structural constraints on the geologic history of eastern Tharsis Rise, Mars, *Icarus*, 284, 43-
973 58, doi:http://dx.doi.org/10.1016/j.icarus.2016.09.005.

974 Wolery, T. J., K. J. Jackson, W. L. Bourcier, C. J. Bruton, B. E. Viani, K. G. Knauss, and
975 J. M. Delany (1990), Current Status of the EQ3/6 Software Package for Geochemical Modeling,
976 in *Chemical Modeling of Aqueous Systems II*, edited, pp. 104-116, American Chemical Society,
977 doi:doi:10.1021/bk-1990-0416.ch008

978 Wolery, T. J. (1992a), EQ3/6, A Software Package for Geochemical Modeling of
979 Aqueous Systems: Package Overview and Installation Guide (Version 7.0): UCRL-MA-110662-
980 PT-I, *Lawrence Livermore National Laboratory, Livermore, California.* .

981 Wolery, T. J. (1992b), EQ3NR, A Computer Program for Geochemical Aqueous
982 Speciation-Solubility Calculations: Theoretical Manual, User's Guide, and Related
983 Documentation (Version 7.0): UCRL-MA-110662-PT-III *Lawrence Livermore National*
984 *Laboratory, Livermore, California.* .

985 Wray, J. J., S. L. Murchie, S. W. Squyres, F. P. Seelos, and L. L. Tornabene (2009),
986 Diverse aqueous environments on ancient Mars revealed in the southern highlands, *Geology*,
987 37(11), 1043-1046.

988 Wray, J. J., S. L. Murchie, J. L. Bishop, B. L. Ehlmann, R. E. Milliken, M. B. Wilhelm,
989 K. D. Seelos, and M. Chojnacki (2016), Orbital evidence for more widespread carbonate-bearing
990 rocks on Mars, *J. Geophys. Res. E Planets*, 121(4), 652-677, doi:10.1002/2015JE004972.